Nondestructive Light-Initiated Tuning of Layer-by-Layer Microcapsule Permeability

Weinan Xu,[†] Ikjun Choi,[†] Felix A. Plamper,[‡,§] Christopher V. Synatschke,[‡] Axel H. E. Müller,[‡] and Vladimir V. Tsukruk[†,*]

[†]School of Materials Science and Engineering, Georgia Institute of Technology, Atlanta, Georgia 30332, United States, and [‡]Makromolekulare Chemie II and Bayreuther Zentrum fur Kolloide und Grenzflächen, Universität Bayreuth, D-95440 Bayreuth, Germany. [§]Present address: Institute of Physical Chemistry, RWTH Aachen University, 52056 Aachen, Germany.

ABSTRACT A nondestructive way to achieve remote, reversible, light-controlled tunable permeability of ultrathin shell microcapsules is demonstrated in this study. Microcapsules based on poly{[2-(methacryloyloxy)ethyl] trimethylammonium iodide} (PMETAI) star polyelectrolyte and poly(sodium 4-styrenesulfonate) (PSS) were prepared by a layer-by-layer (LbL) technique. We demonstrated stable microcapsules with controlled permeability with the arm number of a star polymer having significant effect on the assembly structure: the PMETAI star with 18 arms shows a more uniform and compact assembly structure. We observed that in contrast to regular microcapsules from linear polymers, the permeability of the star polymer microcapsules could be dramatically altered by photoinduced transformation of the trivalent hexacyanocobaltate ions into a mixture of mono- and divalent ions by using UV irradiation. The reversible contraction of PMETAI star polyelectrolyte arms and the compaction of star polyelectrolytes in the presence of multivalent counterions are considered to cause the dramatic photoinduced changes in microcapsule properties observed here. Remarkably, unlike the current mostly destructive approaches, the light-induced changes in microcapsule permeability are completely reversible and can be used for light-mediated loading/unloading control of microcapsules.

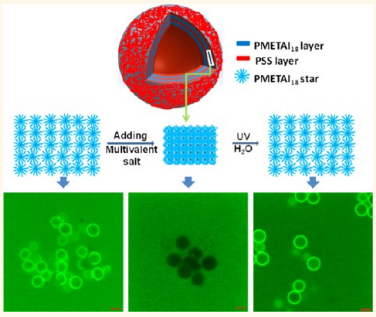

KEYWORDS: layer-by-layer assembly · star polyelectrolyte · tunable microcapsules · shell permeability · salt and UV responsive shells

Responsive materials assembled from nanostructured building blocks have attracted much attention in recent years due to their abilities to adapt and respond to stimuli in surrounding environments.[1] These materials are playing an increasingly important role in fields such as controlled release,[1,2] tissue engineering, biosensors and catalytic systems. Among the many approaches to fabricate responsive polymeric structures, layer-by-layer (LbL) assembly is a highly versatile technique to produce organized structures with desirable properties from many different kinds of materials, such as polymers,[3] nanoparticles,[4] DNA,[5] proteins[6] and viruses.[7,8] Microcapsules prepared *via* LbL techniques have attracted particular interest because their properties can be readily tailored during and after the preparation process.[9,10] In addition, multiple functionalities can be introduced during the stepwise formation, thus creating a novel platform with unprecedented structures and functions.[11,12]

Stimuli-responsive behavior of microcapsules can be achieved in various ways by specific stimuli such as pH, salt, light, ultrasonic and magnetic fields, which can trigger cargo release at the desired location, condition, and time.[13−15] Microcapsules composed of weak polyelectrolytes are generally responsive to the pH of the environment.[16] When the pH of the environment becomes lower (in case of polyacids) or higher (in case of polybases) than the pK_a, the polyelectrolytes become uncharged thus resulting in the increasing permeability.[17] This process can be reversible in most cases when the pH of the environment goes back to the original value.[18] However, the pH responsive approach cannot be remotely controlled, and most of the pH responsive microcapsules are not able to perform satisfactorily in terms of subtle pH change. Another interesting category of responsive microcapsules is magnetic field responsive. By embedding magnetic particles into the polymer shells of microcapsules, the LbL

* Address correspondence to vladimir@mse.gatech.edu.

Received for review October 13, 2012 and accepted December 7, 2012.

Published online December 07, 2012
10.1021/nn304748c

shells can be disturbed, Consequently, this allows the permeation of target molecules through the microcapsule wall,[19] but the long exposure time and strong magnetic field requirement are major challenges.

Light-induced release of polymeric microcapsules has attracted much attention in recent years due to their potential applications in diverse delivery areas.[20] Previous research on light-responsive microcapsules can be divided into three main categories. First, microcapsules may contain metal nanoparticles such as TiO_2,[21] silver,[22] and gold,[23,24] which can either destructively or nondestructively change the permeability and mechanical properties of microcapsules,[25] mostly due to the strong light absorption of the nanoparticles. Unfortunately, the potential toxicity of metal nanoparticles might limit their application in some fields, and most of the approaches are destructive. The second category is microcapsules that contain fluorescent[22] and functional dyes,[26] which can be responsive to visible or IR irradiation. Finally, UV irradiation can change the permeability of microcapsules by photooxidation[27] or optical photoisomerization,[28] but the light responsive properties for these microcapsules are compromised by the fact that only about half of the microcapsules have the ability to encapsulate model substances after UV irradiation. The approaches are destructive to the microcapsules (but not necessarily for the exterior), thus multiple loading−unloading cycles of these microcapsules cannot be completed.

The modulation of the polyelectrolyte microcapsule's permeability by changing the salt concentration in the surroundings is commonly observed for polyelectrolyte-based LbL microcapsules.[20,29,30] The salt-induced permeability change of the microcapsules shell is generated from the shielding of charges on the polyelectrolytes that reduces the interaction between adjacent layers with opposite charges, thus facilitating the diffusion of macromolecules through the multilayer walls. The combination of salt and UV responsive properties can be possibly achieved by using salt with photochemical properties, so that the change in permeability of microcapsule shell induced by the addition of salt can be recovered by decomposing the salt using photochemical reactions. To achieve this goal, the polymers used to compose the microcapsule shell need to be very sensitive to the salt, especially having dramatically different behaviors in the presence of different salt ions before and after the photochemical reaction. Highly branched polyelectrolytes can be considered as the material of choice for the assembly of ion-sensitive shells, among which star polyelectrolytes are excellent candidates for such microcapsules due to their extremely high sensitivity to an ionic environment.[31,32] Compared to dendrimers[33] and other branched polymers,[34,35] star polymers have the advantages of facile synthesis,[36,37] flexible compositions,[38,39] and tunable sizes.[40,41]

There are several pioneering works on microcapsules made from branched polyelectrolyte macromolecules. Poly(amidoamine) dendrimers have been used to prepare hollow capsules by LbL technique with poly(sodium 4-styrenesulfonate) (PSS);[42] however the capsules were unstable toward the core removal procedure and the yield was low. Microcapsules composed of cationic phosphorus dendrimers and PSS were able to selectively encapsulate Cy5 dye molecules *via* DNA hybridization.[43] The mechanical properties of DNA/phosphorus dendrimers-based microcapsules have been studied, and it was found that these microcapsules were softer than microcapsules assembled from linear flexible polyelectrolytes.[44] Hollow microcapsules with a shell constructed entirely from a cationic/zwitterionic pairs of pH-responsive block copolymer micelles have also been successfully prepared, and it was shown that the core/shell structure of the micelles remains intact after LbL assembly.[45]

Herein, we introduce novel LbL microcapsules based on responsive star polyelectrolytes with unique nondestructive, remote, reversible, light-induced tunability of the shell permeability in high contrast with traditional methods which are usually destructive and require adding toxic nanoparticles to the shell composition. Taking advantage of the star polyelectrolyte's unique response to an ionic environment, we can effectively modulate the conformation of PMETAI stars by adding multivalent salt and controlling its state by a mild photoinduced chemical reaction, thus readily tuning the permeability of microcapsules. By using the photochemical reaction, $[Co(CN)_6]^{3-}$, trivalent counterions can be decomposed into monovalent and divalent ions that dramatically affect the conformation of PMETAI star polyelectrolytes and porosity of LbL shells.[46] In contrast to previous approaches, the path suggested here results in reversible, remote, nondestructive light-triggering changes in the permeability of the microcapsules.

RESULTS AND DISCUSSION

The chemical structure of the PMETAI star polyelectrolyte is shown in Scheme 1a. PMETAI is the quaternized ammonium salt of poly{(*N*,*N*-dimethylamino) ethyl methacrylate} (PDMAEMA), which was synthesized by polymerizing DMAEMA by atom transfer radical polymerization employing a core-first strategy. The oligofunctional initiators used here were sugar-based scaffolds as well as silsesquioxane nanoparticles.[47] At very low ionic strength the hydrodynamic radius of $PMETAI_{18}$ is 24 nm, which is about 56% of the contour length of a single arm (42.5 nm), indicating a considerable stretching due to Coulombic repulsion and high osmotic pressure inside the star.[47] As previously reported,[48] when multivalent counterions are added to star polyelectrolyte solution, the arms of the star polyelectrolytes would retract (Scheme 1b). The addition

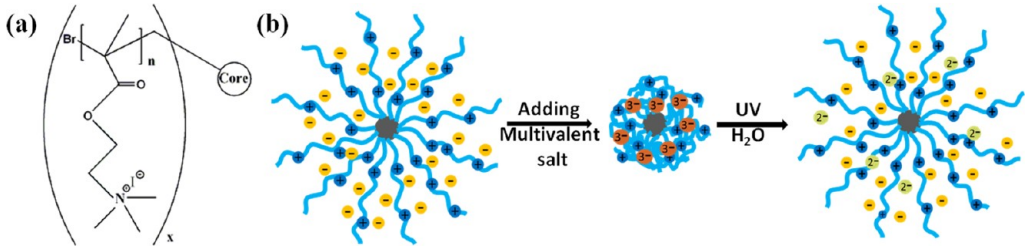

Scheme 1. (a) Chemical structure of PMETAI star polyelectrolyte, (b) structural change of PMETAI after adding $K_3[Co(CN)_6]$ and during the photochemical reaction.

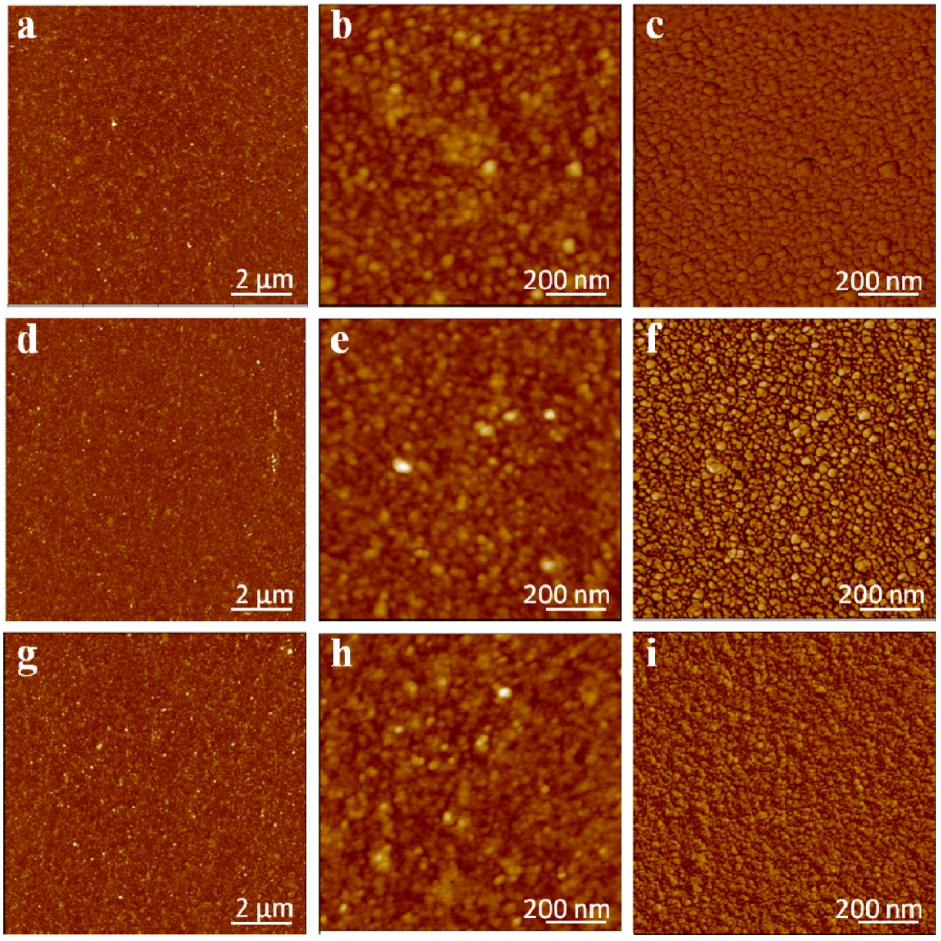

Figure 1. (a–c) AFM images of $(PSS/PMETAI_{18})_5$ film, (d–f) AFM images of $(PSS/PMETAI_{18})_8$ film, (g–i) AFM images of $(PSS/PMETAI_{18})_{11}$ film; panels c, f, and i are phase images. *Z*-scale is 30 nm for topography images and 30° for phase images.

of trivalent hexacyanocobaltate(III) ions leads to the collapse of PMETAI star polyelectrolyte even at low concentrations. Moreover, a PMETAI star can recover to an expanded state from a collapsed state by transforming the trivalent hexacyanocobaltate(III) ions into a mixture of mono- and divalent ions by UV irradiation, as shown in Scheme 1b. Therefore, the conformation and interaction of PMETAI star polyelectrolyte can be switched by controlling the state of multivalent salts with UV irradiation. To take advantage of the unique responsive behaviors of PMETAI star polyelectrolyte and extend its application, we study the properties of planar films first.

$(PSS/PMETAI)_n$ LbL Thin Films. To study the effects of the number of arms of star polyelectrolytes on their self-assembly behavior, two sets of LbL films with 5, 8, and 11 bilayers have been prepared from PSS and 18 and 5.6 armed PMETAI star polyelectrolytes: $(PSS/PMETAI_{18})_n$ and $(PSS/PMETAI_{5.6})_n$. In this designation, for instance, $(PSS/PMETAI_{18})_8$ represents a film (or microcapsule) of eight bilayers made with 18-arm PMETAI star polyelectrolyte.

AFM images of the $PSS/PMETAI_{18}$ films with three different numbers of layers are shown in Figure 1. The films are uniform, which confirms the relatively strong interaction between $PMETAI_{18}$ and PSS components.[49]

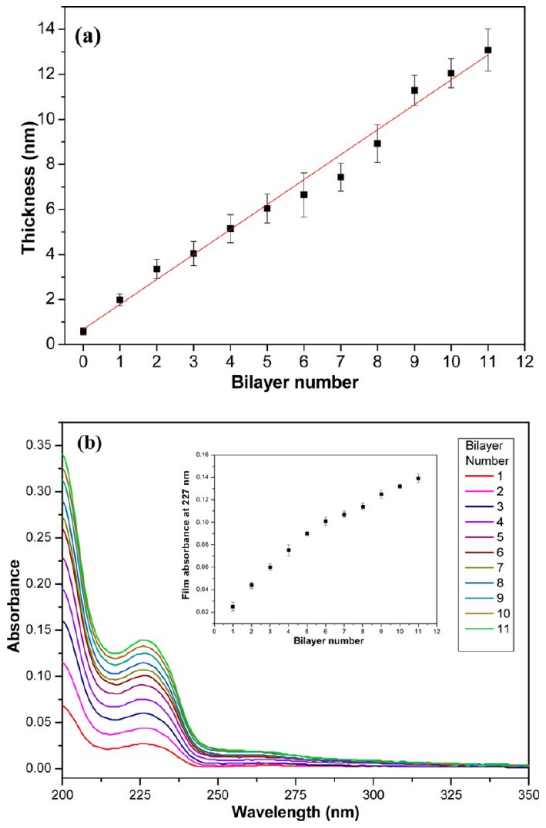

Figure 2. (a) Thickness of $(PSS/PMETAI_{18})_n$ films as a function of bilayer number as measured by ellipsometry. (b) UV−vis spectra of $(PSS/PMETAI_{18})_n$ films with different number of layers assembled on quartz substrate. Inset shows the intensity increase of the peak at 227 nm with bilayer number.

From high resolution AFM topography and phase images, it can be seen that fine granular structures are uniformly distributed throughout the surface. The average size of the granules is below 30 nm, with the height around 2.5 nm, which are close to expected dimensions of PMETAI star polyelectrolytes with extended arms.[48] The density of granule structures on the surface of LbL films gradually increases with the number of layers, while the overall roughness of the films remains almost constant, around 1.7 nm (as measured on 1 × 1 μm area). The microroughness of $(PSS/PMETAI_{18})_n$ films is higher than that of uniform LbL films made by linear polyelectrolytes (usually below 1 nm) due to more pronounced aggregation of star polyelectrolytes.[50]

Figure 2 shows the thickness buildup of $(PSS/PMETAI_{18})_n$ films as obtained from UV absorption and ellipsometry. From UV absorption it is clear that the increase of the number of layers results in a virtually linear growth of film thickness.[51] Both total thickness and the characteristic peak in 227 nm which is attributed to the phenyl ring in PSS linearly increase with the number of layers.

AFM images for the $(PSS/PMETAI_{5.6})_n$ films show different characteristics compared with that of $(PSS/PMETAI_{18})_n$ films (Figure 3). The high resolution AFM topography and phase images of $(PSS/PMETAI_{5.6})_5$ films show uniform distribution of granular aggregates. The average size of these granule structures (below 20 nm) is smaller than that of the 18-arm PMETAI star polyelectrolytes. With the increase of number of layers, some larger-scale aggregation occurs as can be clearly seen for 8 and 11 bilayer films. This process is confirmed by the increased microroughness of $(PSS/PMETAI_{5.6})_n$ films with 5, 8, and 11 bilayers from 1.1 to 2.2, and 3.9 nm, respectively.

Despite the appearance of larger aggregates on the film surface, the average thickness of $(PSS/PMETAI_{5.6})_n$ films grows linearly with layer number, as proven by the thickness data from ellipsometry measurement (Supporting Information, Figure S1a). The UV absorbance intensity at 227 nm increases almost linearly with increasing layer number (Figure S1b) indicating consistent growth of LbL films. For the same number of layers, the $(PSS/PMETAI_{5.6})_n$ film is slightly thinner than the $(PSS/PMETAI_{18})_n$ film, due to the lower molecular weight of 5.6-arm star polymer.[47]

Morphology of $(PSS/PMETAI)_n$ LbL Microcapsules. The common preparation routine for $(PSS/PMETAI)_n$ microcapsules is shown in Scheme 2.[11,52] Similar to $(PSS/PMETAI)_n$ films, we also prepared LbL microcapsules using two different PMETAI star polyelectrolytes with 5.6 arms and 18 arms and with 5, 8, and 11 bilayer shells.

An electrophoresis experiment was conducted to monitor the LbL growth of PSS and PMETAI star polyelectrolytes. As shown in Figure 4, the ζ-potential of bare silica particles was *ca.* −70 mV. A ζ-potential of *ca.* −75 mV was obtained for microcapsules when PSS was the outmost layer of film on silica core. On the other hand, a positive ζ-potential of +72 mV was observed when $PMETAI_{18}$ star polyelectrolyte was the outmost layer. On the whole, the alternating surface charge of coated silica particles was strong evidence that consistent LbL assembly of anionic PSS and cationic PMETAI components took place during the fabrication process.[53,54]

SEM images of $(PSS/PMETAI_{18})_{11}$ and $(PSS/PMETAI_{5.6})_{11}$ microcapsules are shown in Figure 5. SEM images of the microcapsules based on PMETAI star polyelectrolyte and PSS with five and eight bilayers are shown in Supporting Information, Figures S2 and S3; it can be seen that all of the different kinds of microcapsules are uniform in size. The average thicknesses for $(PSS/PMETAI_{18})$ microcapsules with 5, 8, and 11 bilayers are 12.8, 16.1, and 21.6 nm, respectively, which is higher than that of planar films with the same number of layer (see comparison in Figure 6a). The average bilayer thicknesses of $(PSS/PMETAI_{18})_n$ films and microcapsules in dry state are 1.2 and 2.0 nm, respectively. The rougher silica particles resulted in larger adsorbed amount as discussed in earlier reports.[55]

Stable and monodisperse microcapsules were produced upon removal of silica cores, although a certain

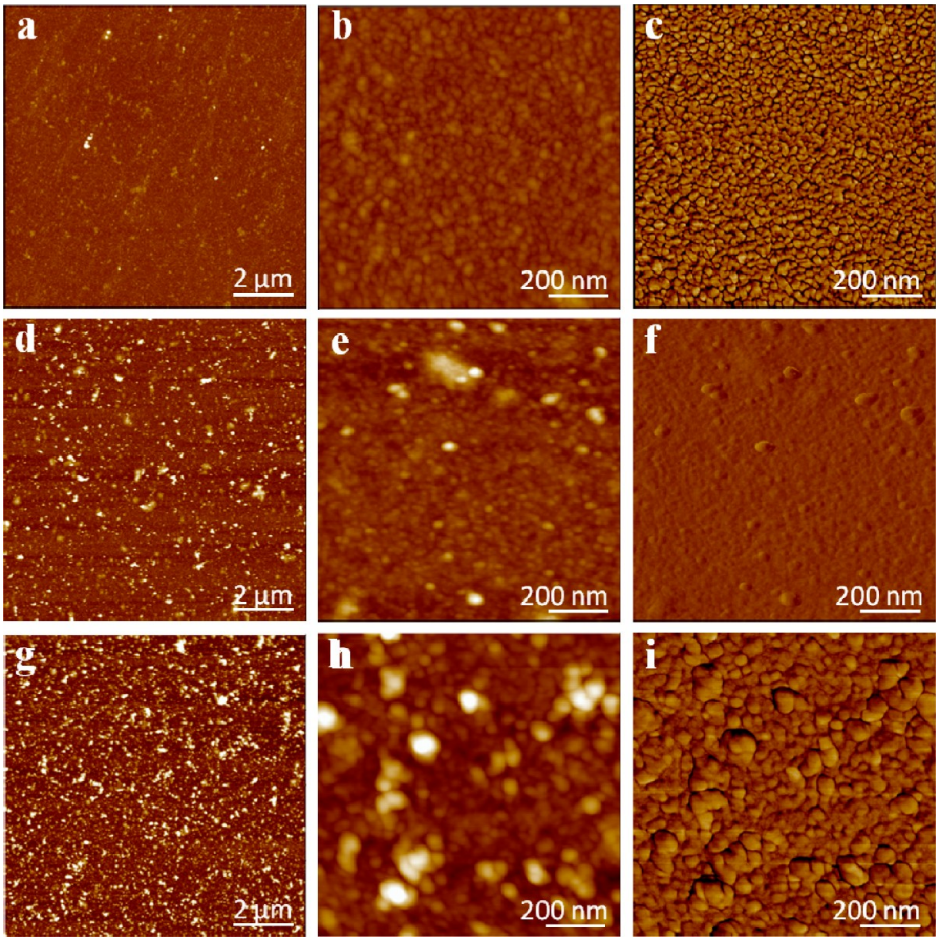

Figure 3. (a–c) AFM images of $(PSS/PMETAI_{5.6})_5$ film, (d–f) AFM images of $(PSS/PMETAI_{5.6})_8$ film, (g–i) AFM images of $(PSS/PMETAI_{5.6})_{11}$ film; panels c, f, and i are phase images. *Z*-scale is 30 nm for topography images and 30° for phase images.

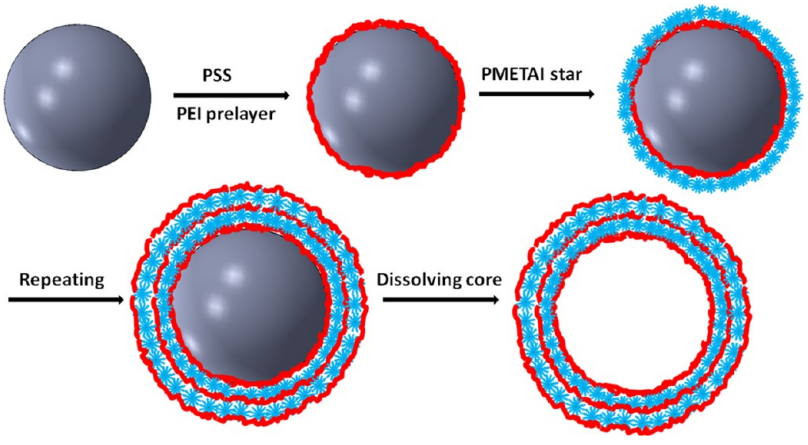

Scheme 2. LbL assembly on silica core and fabrication of $(PSS/PMETAI)_n$ hollow microcapsule.

amount of shrinkage was observed. From confocal microscopy images it can be seen that the average diameter of hollow $(PSS/PMETAI)_n$ microcapsules was 3.0 μm, compared with a 4.0 μm diameter of the original silica particles. Such shrinkage of microcapsules based on highly branched polymers is in accordance with previous research and is related to partial collapse of the inner porous network upon core removal.[56]

Figure 7 shows AFM images of dried $(PSS/PMETAI_{18})_n$ hollow microcapsules with 5, 8, and 11 bilayers. The large scale images show that the microcapsules are quite robust even after drying, preserve their near spherical shape, and avoid aggregation due to strong Coulombic repulsion. Characteristic grainy morphology with occasional wrinkles and folded shells is visible for all three microcapsules with different number of layers.

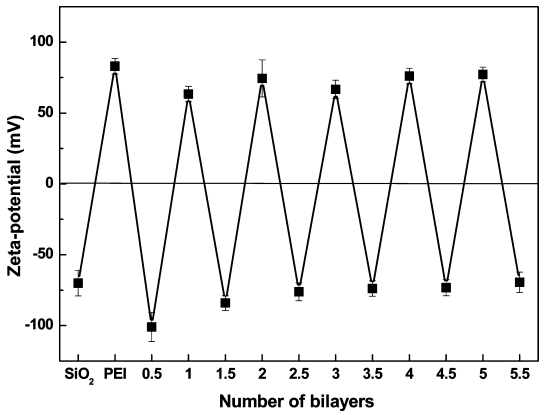

Figure 4. Zeta (ζ)-potential as a function of bilayer number during LbL coating of silica particles with alternating (PSS/PMETAI$_{18}$) bilayers.

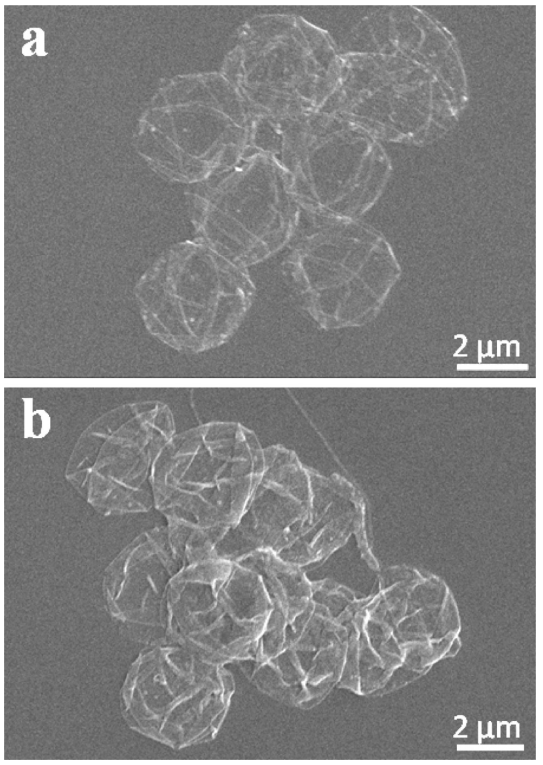

Figure 5. SEM images of (PSS/PMETAI$_{18}$)$_{11}$ (a) and (PSS/PMETAI$_{5.6}$)$_{11}$ (b) microcapsules.

Similar to the morphology of films, high density of grains is visible with uniform distribution of aggregated nanostructures, a common feature for LbL shells with weakly interacting components.[57,58] The overall microroughness of (PSS/PMETAI$_{18}$)$_n$ microcapsules is higher than that of films (see Figure 6b) with the microroughness of microcapsules with 5, 8, and 11 bilayers increasing to 2.3, 2.8, and 3.6 nm, respectively.

Figure 8 shows the AFM images of (PSS/PMETAI$_{5.6}$)$_n$ microcapsules with 5, 8, and 11 bilayers. The thickness of microcapsules with 5, 8, and 11 bilayers is 12.4, 14.8, and 17.1 nm, respectively (Figure 6a). Similar to that of (PSS/PMETAI$_{5.6}$)$_n$ films, high resolution topography and

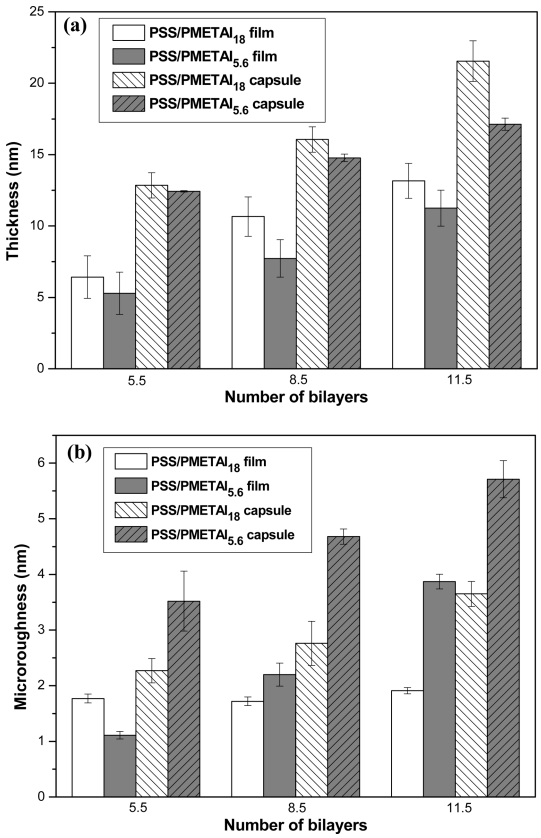

Figure 6. (a) Comparison of thickness of (PSS/PMETAI$_{18}$)$_n$ with (PSS/PMETAI$_{5.6}$)$_n$ for both microcapsules and films. (b) Comparison of microroughness of (PSS/PMETAI$_{18}$)$_n$ and (PSS/PMETAI$_{5.6}$)$_n$ for microcapsules and films.

phase images of microcapsules show a grainy surface morphology, increased porosity, as well as larger-scale aggregation. Such an aggregation significantly increases the microroughness of microcapsules as compared with that of (PSS/PMETAI$_{18}$)$_n$, and indicates less regular LbL growth. The microroughness of (PSS/PMETAI$_{5.6}$) microcapsules with 5, 8, and 11 bilayers is 3.5, 4.7, and 5.7 nm, respectively (Figure 6b). We suggest that the higher microroughness of these microcapsules and increasing porosity might affect the permeability of the microcapsules, as will be discussed in the following section.

Controlled Permeability of (PSS/PMETAI)$_n$ Microcapsules. Fluorescein isothiocyanate (FITC)−labeled dextrans of various molecular weights were used as fluorescent probes to study the permeability of microcapsules with confocal microscopy (Table 1).[16,59] As expected for diffusion controlled processes, the permeability of microcapsules decreases with the increase of layer number.[60] For (PSS/PMETAI$_{18}$) microcapsules with five and eight bilayers, FITC-dextran with a molecular weight of 2000 kDa and below is able to permeate through the shells. For (PSS/PMETAI$_{18}$)$_{11}$ microcapsules, FITC-dextran with a molecular weight of 500 kDa and below can permeate through the shells, while 2000 kDa FITC-dextran cannot.

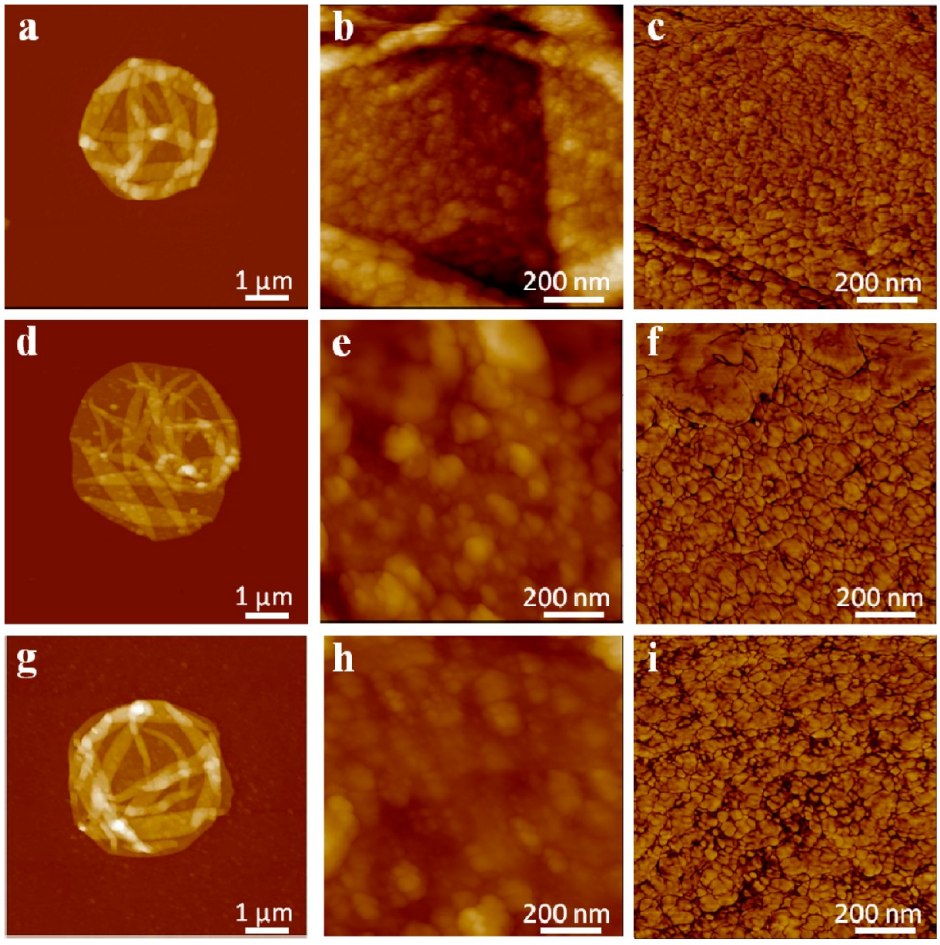

Figure 7. (a−c) AFM images of $(PSS/PMETAI_{18})_5$ microcapsule, (d−f) AFM images of $(PSS/PMETAI_{18})_8$ microcapsule, (g−i) AFM images of $(PSS/PMETAI_{18})_{11}$ microcapsule; panels c, f, and i are phase images. *Z*-scale is 200 nm for topography images and 80° for phase images.

Confocal microscopy images of $(PSS/PMETAI_{18})_{11}$ microcapsules with different molecular weight FITC-dextran are shown in Figure 9. Images for microcapsules with five and eight bilayers are shown in Supporting Information, Figures S5 and S6, respectively. For $(PSS/PMETAI_{5.6})_n$ microcapsules, the confocal microscopy images of capsules with different number of layers are shown in Supporting Information, Figure S7, with the shells of the capsules labeled with FITC for clarity. It can be seen that $(PSS/PMETAI_{5.6})_n$ microcapsules with a different number of layers are also very stable and uniform during a change in the environment of the surrounding.

Considering that the reported hydrodynamic diameters of 2000 kDa and 500 kDa FITC-dextran are 53.8 and 31.8 nm,[61] respectively, the mesh size of $(PSS/PMETAI_{18})_5$, $(PSS/PMETAI_{18})_8$ and $(PSS/PMETAI_{18})_{11}$ shells should fall within the 30−50 nm range. This result is in accordance with a previous permeability study of microcapsules with very thin shells and from weak hydrogen-bonded components or proteins.[18,62] On the other hand, these pore sizes are much larger than the common pore dimensions for conventional polyelectrolyte-based LbL shells (a few nanometers across).[52]

The incorporation of branched polyelectrolytes in LbL shells, which are known to exhibit conformational changes in the presence of counterions, has been exploited to tune the permeability of microcapsules.[63] Indeed, previous studies showed that the addition of trivalent ions (La^{3+}) might lead to a collapsed polyelectrolyte brush, which is caused by a reduction of the interior osmotic pressure.[64,65] Plamper *et al.*[48] demonstrated that the arms of the cationic star polyelectrolyte (which is also 18-armed PMETAI) retract when multivalent counterions are added and that trivalent hexacyanocobaltate (III) ions lead to the collapse of $PMETAI_{18}$ stars even at very low concentrations. Molecular dynamic simulations and AFM observations have also shown that the dendrimers and star polymers can collapse upon the addition of multivalent salt ions.[66−68]

In this study, adding hexacyanocobaltate (III) ions ($[Co(CN)_6]^{3-}$) to the solution of $(PSS/PMETAI_{18})_n$ microcapsules was used to tune the permeability of microcapsule shells. First, we found that before adding $K_3[Co(CN)_6]$ to the solution, $(PSS/PMETAI_{18})_n$ microcapsules showed a high permeability. Figure 9 panels e and f show the confocal microscopy images of $(PSS/PMETAI_{18})_{11}$

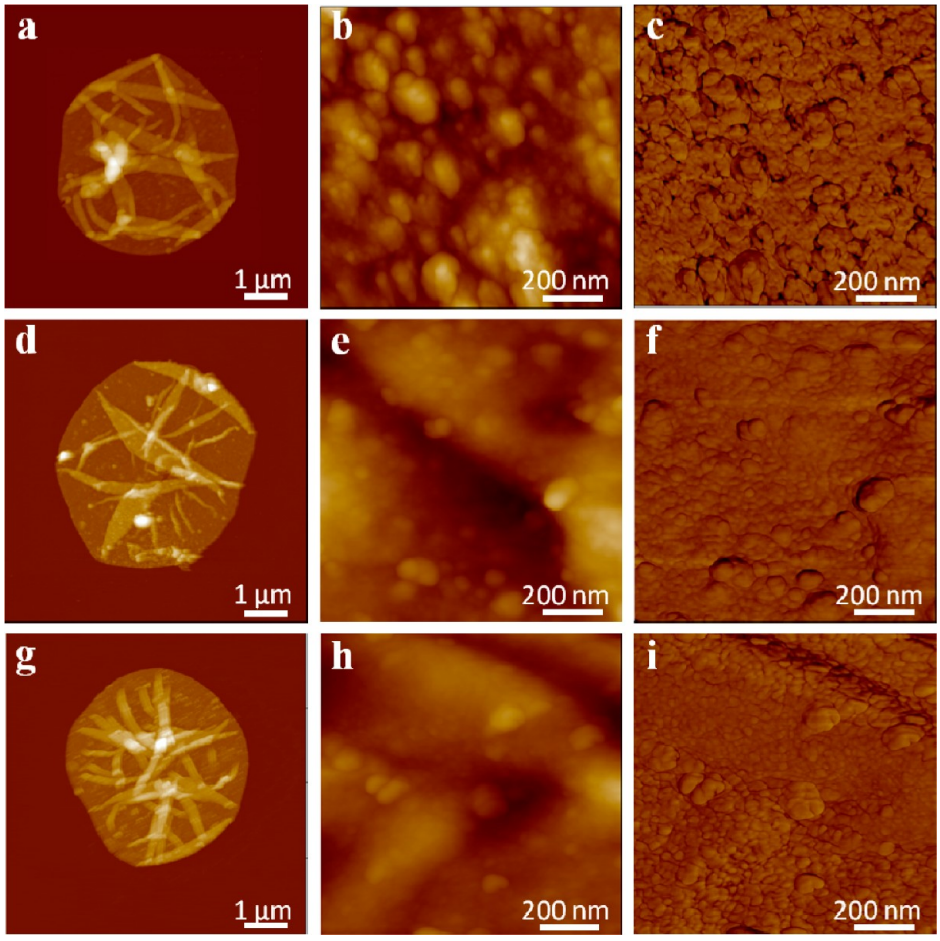

Figure 8. (a–c) AFM images of $(PSS/PMETAI_{5.6})_5$ microcapsule, (d–f) AFM images of $(PSS/PMETAI_{5.6})_8$ microcapsule, (g–i) AFM images of $(PSS/PMETAI_{5.6})_{11}$ microcapsule; panels c, f, and i are phase images. *Z*-scale is 200 nm for topography images and 80° for phase images.

TABLE 1. Permeability of $(PSS/PMETAI_{18})_n$ Microcapsules to FITC-Dextrans with Different Molecular Weight ("+": Permeable, "—" nonpermeable)

sample	FITC-Dextra 70 kDa	FITC-Dextra 250 kDa	FITC-Dextra 500 kDa	FITC-Dextra 2000 kDa
$(PSS/PMETAI_{18})_5$ in buffer	+	+	+	+
$(PSS/PMETAI_{18})_5$ after adding 0.8 mM $K_3[Co(CN)_6]$	—	—	—	—
$(PSS/PMETAI_{18})_8$ in buffer	+	+	+	+
$(PSS/PMETAI_{18})_8$ after adding 0.8 mM $K_3[Co(CN)_6]$	—	—	—	—
$(PSS/PMETAI_{18})_{11}$ in buffer	+	+	+	—
$(PSS/PMETAI_{18})_{11}$ after adding 0.8 mM $K_3[Co(CN)_6]$	—	—	—	—

microcapsules with 500 kDa and 70 kDa FITC-dextran after adding $K_3[Co(CN)_6]$, respectively. After adding trivalent salt ions at a concentration of 0.8 mM, the permeability of $(PSS/PMETAI_{18})_n$ microcapsules dramatically decreases with threshold level decreasing to a molecular weight of 70 kDa. Considering that the hydrodynamic diameter of 70 kDa dextran is around 13.0 nm, we can conclude that the pore dimensions of the $(PSS/PMETAI_{18})_n$ shells were reduced by a factor of 3 under these conditions. Additionally, the average size of the $(PSS/PMETAI_{18})_n$ microcapsules in the solution state decreased from 3.0 to 2.6 μm after adding 0.8 mM trivalent salt, thus further confirming densification of the shells.

On the other hand, the concentration of $K_3[Co(CN)_6]$ also plays an important role in the permeability of $(PSS/PMETAI_{18})_n$ microcapsules. At very low concentration (<0.1 mM) the permeability of $(PSS/PMETAI_{18})_8$ only decreases by a small extent, so that less 500 kDa FITC-dextran can diffuse across the shell (Figure 10b). At the $K_3[Co(CN)_6]$ concentration of around 0.8 mM, $(PSS/PMETAI_{18})_8$ microcapsules are impermeable for 500 kDa FITC-dextran (Figure 10c). If the concentration of added $K_3[Co(CN)_6]$ is further increased, for instance

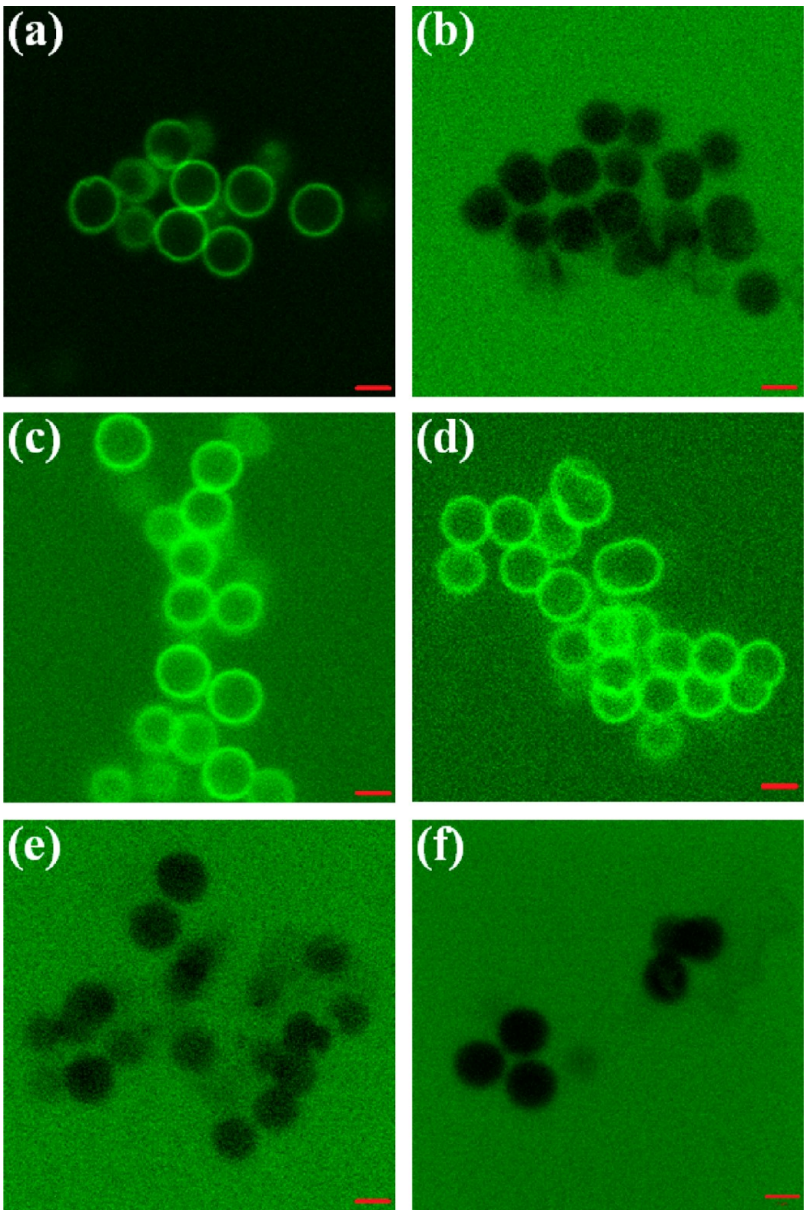

Figure 9. Confocal images of $(PSS/PMETAI_{18})_{11}$ microcapsules exposed to FITC (a), and FITC-dextran solutions with M_w of 2000 kDa (b), 500 kDa (c), 70 kDa (d). After adding 0.8 mM $K_3[Co(CN)_6]$, $(PSS/PMETAI_{18})_{11}$ microcapsules exposed FITC-dextran solutions with M_w of 500 kDa (e), 70 kDa (f). Scale bar is 2 μm.

to 4 mM, the effect in closing the pores of $(PSS/PMETAI_{18})_n$ capsules decreases and shells become permeable to a certain extent (Figure 10d).

These changes in shell permeability can be understood considering well-known results for polyelectrolyte solutions.[48,64,67−70] For instance, it has been demonstrated that the presence of multivalent ions leads to attraction between planar polyelectrolyte brushes and similarly charged polyelectrolytes.[71,72] As is known, adding multivalent salt to the solution of star polyelectrolytes causes collapse of the star conformation if the salt concentration exceeds a critical value and the collapsed state can re-expand if the salt concentration increases beyond a second critical value (reentrant condensation).[73] At very low ionic strength the arms of $PMETAI_{18}$ star polyelectrolytes are nearly stretched to full length,[74] and after LbL assembly of PSS and $PMETAI_{18}$, $PMETAI_{18}$ could maintain the stretched conformation, since the interpenetration between layers happens to a low extent. For star polyelectrolyte like $PMETAI_{18}$, the correlation with counterions has proven to be much stronger, so that the counterions are mostly localized within the shells which are composed of arms.[64] The strong binding of polyelectrolyte with counterions is accompanied by a significantly reduced osmotic activity of the counterions, thus creating high osmotic pressure within star polyelectrolytes, as a result, the arms of PMETAI stars should be strongly stretched.

The conformation of star polyelectrolytes is largely controlled by the balance between osmotic pressure of

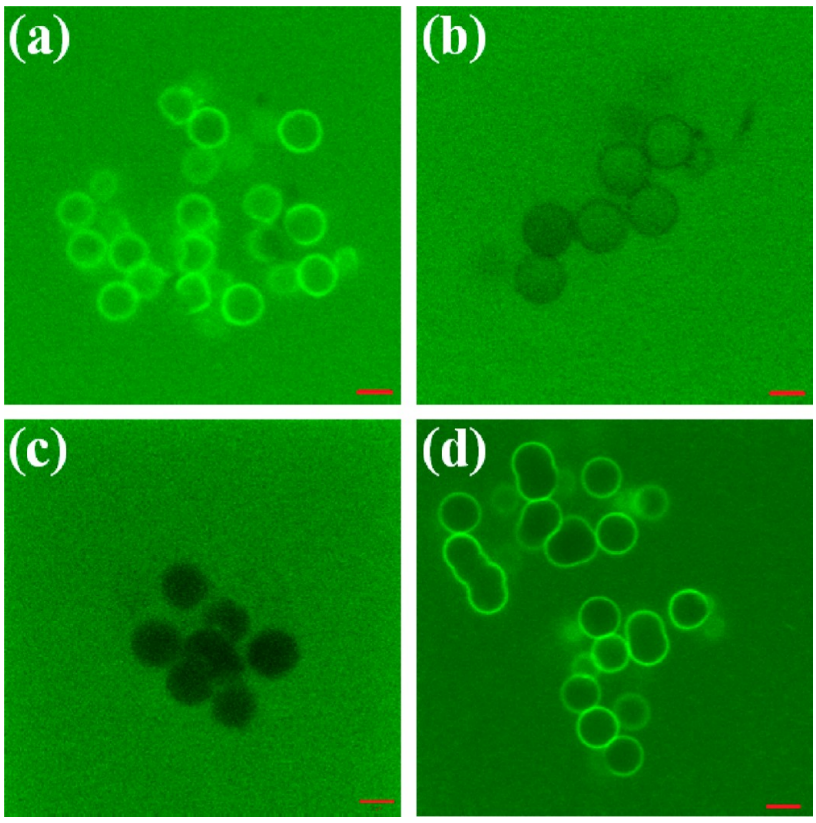

Figure 10. Permeability of $(PSS/PMETAI_{18})_8$ microcapsules to 500 kDa FITC-dextran after adding $K_3[Co(CN)_6]$: (a) without $K_3[Co(CN)_6]$, (b) 0.08 mM, (c) 0.8 mM, (d) 4 mM of $K_3[Co(CN)_6]$. Scale bar is 5 μm.

the entrapped counterions and the arm elasticity.[32] Upon the addition of $K_3[Co(CN)_6]$, the monovalent counterions I^- are replaced by $[Co(CN)_6]^{3-}$. On average three I^- ions are replaced by one $[Co(CN)_6]^{3-}$, with the ion exchange process controlled by the Donnan effect.[64] Thus the osmotic pressure inside $PMETAI_{18}$ is reduced by a factor of three and a strong shrinking of the arm stretching and a collapse occur. Previous study showed that star polyelectrolytes collect multivalent counterions from the surroundings until they become saturated, so that the collapse of star polyelectrolytes begins at quite a low salt concentration.[64] In our system, we use a relatively low concentration of $PMETAI_{18}$ solution (0.2 mg/mL) to perform LbL assembly, and after the assembly process, the actual $PMETAI_{18}$ concentration would be even lower. Therefore, a very low concentration of $K_3[Co(CN)_6]$ should be enough to make the $PMETAI_{18}$ star polyelectrolyte effectively collapse.

The interaction of $PMETAI_{18}$ star polyelectrolytes within swollen shells is mediated by three factors: the electrostatic interactions, steric repulsion between arms, and the entropic repulsion of counterions. It has been proven that entropic repulsion of the counterions is the dominant force between two star polyelectrolytes.[70] During the collapse of $PMETAI_{18}$ star polyelectrolytes upon adding $[Co(CN)_6]^{3-}$, the steric stabilization effect also breaks down. The interaction between PSS and $PMETAI_{18}$ decreases because $[Co(CN)_6]^{3-}$ compensates a great portion of positive charges on $PMETAI_{18}$ arms. What's more, the contraction of $PMETAI_{18}$ arms would decrease the number of attraction sites between PSS and $PMETAI_{18}$. On the other hand, due to the presence of $[Co(CN)_6]^{3-}$ ions between $PMETAI_{18}$ stars, there is an attraction force between the star polyelectrolytes. The concentration of counterions surrounding the $PMETAI_{18}$ star molecules also decreases heavily due to the replacement of I^- ions with $[Co(CN)_6]^{3-}$ ions. Therefore, the entropic repulsion between counterions decreases, which also contributes to the attraction between stars with added $K_3[Co(CN)_6]$.

We suggest that the collapse of the arm chains and the attraction between $PMETAI_{18}$ stars jointly contribute to the significant decrease in the permeability of $(PSS/PMETAI_{18})_n$ shells with salt concentration changes. On the other hand, the pore size is largely determined by the space between arms of the $PMETAI_{18}$ stars packed in shells (Scheme 3).[75] Upon addition of the $K_3[Co(CN)_6]$ salt, the contraction of $PMETAI_{18}$ stars significantly decreases the distance between the arms. At the same time, the increasing attractive forces between $PMETAI_{18}$ stars make them migrate closer, thus the molecular packing become denser. As a result, the pore size as well as the overall size of the microcapsule decreases, which corresponds to the permeability measurements. The small angle neutron scattering

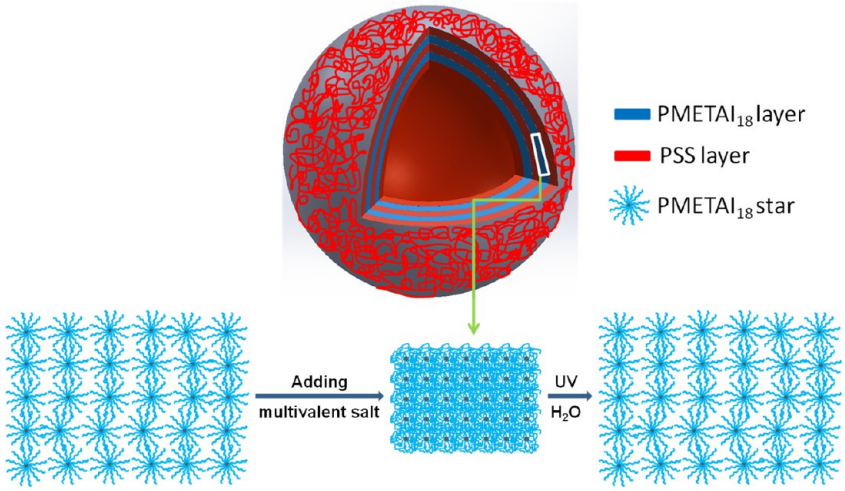

Scheme 3. Responsive behavior of $(PSS/PMETAI_{18})_n$ microcapsules to multivalent salt and UV irradiation.

experiments are in progress to further elucidate this behavior.

As suggested, the most contracted structure of star polyelectrolytes appears when the total charge of multivalent counterions neutralizes the polyelectrolyte charge.[69] When the multivalent salt concentration increases beyond that point, the arms start to expand again. In contrast, in the presence of monovalent counterions, star polyelectrolytes exhibit a slow, monotonic decrease of radius of gyration with the increase of salt concentration. Arm re-expansion is linked to charge reversal,[76] when the arms of $PMETAI_{18}$ stars are filled with $[Co(CN)_6]^{3-}$ ions, the repulsion between these ions induces the separation of arms. Therefore, at relatively high $K_3[Co(CN)_6]$ salt concentration when the $PMETAI_{18}$ stars re-expand, the space between arms of $PMETAI_{18}$ as well as the intermolecular distances increase, so that the shell permeability also increases. Thus, if external stimuli can affect the ion state inside shells, the permeability and thus loading–unloading behavior of microcapsules can be tuned on-demand, this intriguing possibility is further discussed below.

UV Triggered Release of $(PSS/PMETAI_{18})_n$ Microcapsules. In our next effort, we took advantage of the simple and well-known photochemical behavior of a cyanide complex; $[Co(CN)_6]^{3-}$ ions can be converted into monovalent and divalent ions with UV irradiation according to the reaction[46]

$$Co(CN)_6^{3-} \xrightarrow[H_2O]{h\nu} Co(CN)_5(H_2O)^{2-} + CN^-$$

This photoaquation reaction has a quantum yield of 0.31 at 25 °C independent of the wavelength of irradiation (254, 313, and 365 nm), the concentration of the complex, and the pH of the solution (2.0–7.5). It has also been demonstrated that the thermal reaction opposed to the photoaquation was not appreciable.[77] The photochemical reaction could complete in about 30 min under normal illumination conditions.[46] The decomposition of $[Co(CN)_6]^{3-}$ ions into $[Co(CN)_5]^{2-}$ and CN^- results in the total number of counterions increasing dramatically, so that the osmotic pressure within $PMETAI_{18}$ stars becomes much higher. Moreover, the entropic repulsion between counterions also increases at higher concentration, which also contributes to a stretched conformation of arms.

To explore this possibility to tune the state of LbL shells, the suspension of $(PSS/PMETAI_{18})_n$ microcapsules was irradiated using a UVP B-100A high powered UV lamps (100 W) at a wavelength of 365 nm. The samples were placed in quartz cuvettes and then immersed in a cooled water bath, which was placed 7 cm away from the lamp. First, we observed that $(PSS/PMETAI_{18})_8$ microcapsules are impermeable to 500 kDa FITC–dextran after adding 0.8 mM $K_3[Co(CN)_6]$ (Figure 11). However, after UV irradiation for 45 min, these microcapsules become permeable to 500 kDa dextran again.

To further explore the role of the multivalent salt and UV irradiation on the permeability of $(PSS/PMETAI_{18})_n$ microcapsules, we also conducted loading–unloading test. For this test, 500 kDa FITC-dextran was added to the solution of $(PSS/PMETAI_{18})_n$ microcapsules and it permeated quickly into microcapsules. Then $K_3[Co(CN)_6]$ was added to the solution to reach a concentration of 0.8 mM, so that the pores on the wall of capsules became effectively closed thus trapping the labeled dextran. Subsequently, FITC-dextran outside of the capsules was removed by several centrifugation and washing steps and replaced with pure water. Thus, encapsulation of 500 kDa FITC-dextran was achieved in this way with fluorescent FITC-dextran encapsulated inside $(PSS/PMETAI_{18})_8$ microcapsules as confirmed by confocal microscopy (Figure 11c).

On the other hand, the encapsulated FITC-dextran can be released by initiating pore opening with UV irradiation based on the mechanism discussed above (Figure 11d). After UV irradiation for 45 min, FITC-dextran encapsulated within the $(PSS/PMETAI_{18})_8$

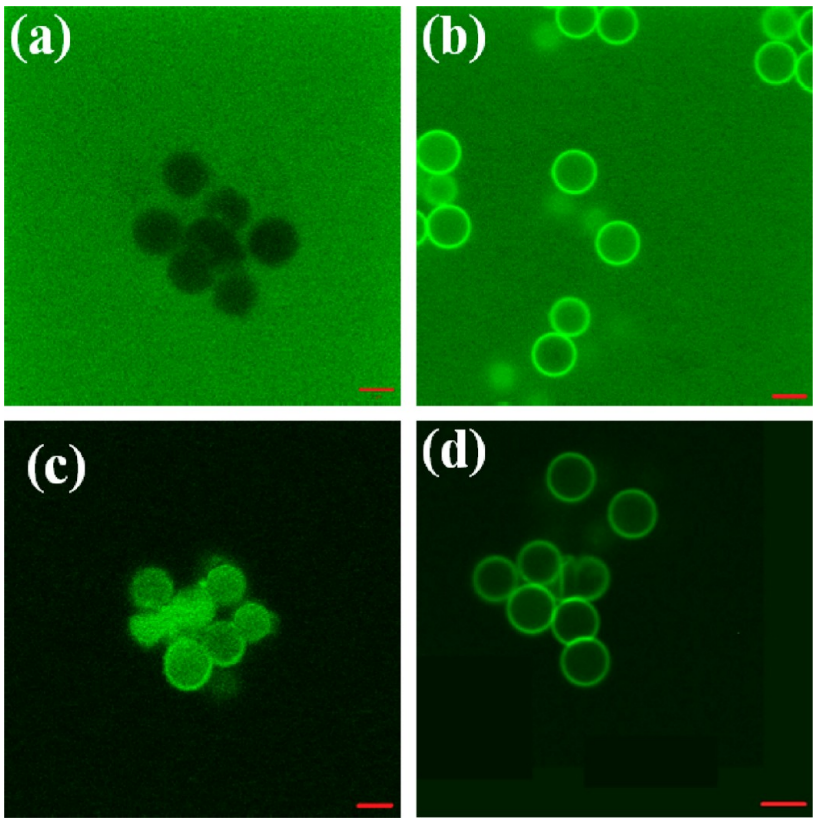

Figure 11. Permeability of $(PSS/PMETAI_{18})_8$ microcapsules to 500 kDa FITC-dextran, (a) after adding 0.8 mM $K_3[Co(CN)_6]$, (b) add 0.8 mM $K_3[Co(CN)_6]$, then irradiate by UV for 45 min; (c) encapsulation of 500 kDa FITC-dextran by adding 0.8 mM $K_3[Co(CN)_6]$; (d) release of FITC-dextran by 45 min UV irradiation.

microcapsules was released, so that both the background and microcapsule interior are dark. Only the microcapsule shells remain fluorescent due to the residual FITC-dextran. To exclude the possibility of excessive photobleaching, we also conducted a control experiment, which is shown in Supporting Information, Figure S8. The fluorescence intensity inside the microcapsules is a direct evidence of the existence of the probe molecules.[56] Before adding $K_3[Co(CN)_6]$ to the suspension, the microcapsule interior is nearly as bright as the background, which shows that FITC-dextran can easily permeate into the microcapsules. After trivalent salt was added, pores on the microcapsule shells are largely closed, so that the microcapsule interior would still be bright due to encapsulated FITC-dextran and the background would be dark after removing surrounding dye molecules.

The encapsulation efficiency can be estimated by the ratio of the average fluorescence intensity of microcapsule interior before and after removing the labeled dextran from exterior. This intensity comparison shows that around 84% of FITC-dextran was successfully encapsulated. This encapsulation and release cycle can be repeated with high efficiency multiple times by alternatively adding $K_3[Co(CN)_6]$ salt and UV irradiation (Supporting Information, Figure S9). The encapsulation efficiency as measured in the ratio of fluorescent intensities remains high and stable over multiple cycles of UV-irradiation followed by ion additions (Figure 12).

The phenomenon demonstrated here can be compared to several existing approaches to remotely control shell permeability of LbL microcapsules with light. One of the popular approaches incorporated metal nanoparticles like gold or silver into shells which absorb the light energy. The heat produced by nanoparticles can be harvested to release encapsulated substances from microcapsules, which are shown to be viable and applicable even for intracellular release. But at high nanoparticle content, the microcapsules are less stable and the responsiveness to light also decreases.[78] Next, UV responsive polymer core−shell micelles were developed as nanocarriers, with the micelle core-forming hydrophobic block containing a photolabile chromophore as a pendant group.[79] Upon UV irradiation, the chemical bond breaks detaching the chromophore from the polymer and transforming the hydrophobic block into a hydrophilic block, which leads to the dissociation of polymer micelles. Compared to our approach, due to the small size of polymer micelles (around 15 nm), they have much lower loading capacity and their dissociation is irreversible. Another approach is utilizing macromolecules containing photoisomerizable azobenzene moieties.[28] These microcapsules can shrink and encapsulate fluorescently labeled polymers, and the permeability decreases

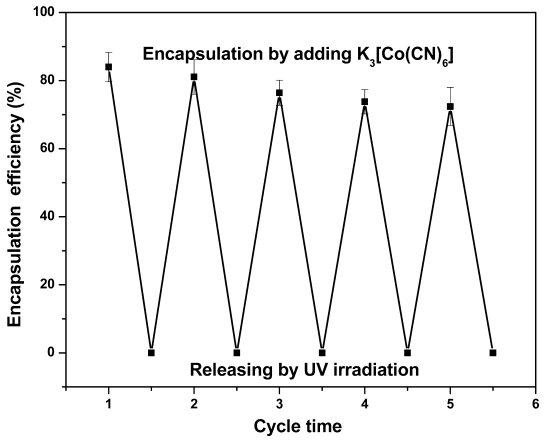

Figure 12. Encapsulation efficiency (defined by the ratio of average fluorescence intensity of microcapsule interior before and after removing surrounding dye) *versus* repeatable UV irradiation cycles.

upon UV irradiation; however, the permeability change was found to be irreversible. Therefore, light-stimulated loading−unloading ability based upon the internal ion state control suggested here is very different from previous mostly destructive approaches and provides a much more efficient path for remote, reversible, cyclical tuning of shell permeability without the drawbacks of most current approaches.

CONCLUSIONS

LbL films and microcapsules based on PMETAI star polyelectrolytes were successfully assembled and explored as efficient cargo carriers with light-induced remote control of shell permeability, and capable of multiple and reversible loading−unloading behavior. This novel "soft" path in contrast to current mostly destructive approaches is based upon light-initiated ionic state transformation, which affects the porosity of shells composed of ion-sensitive star polyelectrolytes. The permeability of $(PSS/PMETAI_{18})_n$ shells can be significantly reduced by adding a small amount of $K_3[Co(CN)_6]$ salt to the suspension due to a collapse of PMETAI stars, causing a dramatic reduction in the pore size. Then $K_3[Co(CN)_6]$ salt can be decomposed into monovalent and divalent ions by UV irradiation, so that the permeability and dimension of $(PSS/PMETAI_{18})_n$ microcapsules can be recovered. The responsive properties of microcapsules also prove that star polyelectrolytes could retain their stimuli-responsive character after incorporating within LbL system, which is in accordance with previous reports.[80−83]

The light-induced changes in microcapsule permeability demonstrated here are completely reversible and can be used for light-mediated loading−unloading behavior of LbL microcapsules in contrast to current microcapsule-destructive approaches. UV-responsive microcapsules composed of star polyelectrolytes offer a uniquely adaptive and tunable way of cargo delivery and unloading which could find applications in sustained release, controlled delivery, microreactors, and catalytic systems.

EXPERIMENTAL SECTION

Materials. Poly(ethylene imine) (PEI) was purchased from Polysciences. PSS (M_w = 70K) and poly(allylamine hydrochloride) (PAH, M_w = 58K) were purchased from Sigma-Aldrich. All commercial polyelectrolytes were used without further purification. Potassium hexacyanocobaltate (III) was also purchased from Sigma-Aldrich, with a total impurity ≤0.1%. Silica particles with a diameter of 4.0 ± 0.2 μm and 10% dispersion in water were obtained from Polysciences. Hydrofluoric acid (48−51%) was purchased from BDH Aristar. Nanopure water (Nanopure system, Barnstead) with a resistivity of 18.2 MΩ cm was used in all experiments.

Synthesis of PMETAI Star Polyelectrolytes. Poly{[2-(methacryloyloxy)-ethyl] trimethylammonium iodide} (PMETAI) is the quaternized ammonium salt of poly[2-(*N*,*N*-dimethylamino)ethyl methacrylate] (PDMAEMA). PDMAEMA was synthesized by atom transfer radical polymerization employing a core-first approach.[47] Sugar-based scaffolds as well as silsesquioxane nanoparticles were used as oligofunctional initiators. The rather low efficiency of the initiation sites (30−75%) leads to a moderate arm number distribution of the prepared polyelectrolyte stars. For quaternization, PDMAEMA was dissolved in acetone and methyl iodide was added at room temperature at a molar ratio of 1.5 compared to amino groups. The mixture was kept stirring overnight to ensure quantitative conversion. Acetone was decanted, and the polymer was washed several times with acetone. Then quaternized polymer was dissolved in water and dialyzed against pure water for 2 days and finally freeze-dried. Here we used star PMETAI with an arm number of 18 (number average, polydispersity index (PDI) in arm number distribution ≈ 1.4) and a number-average degree of polymerization per arm of 170 (PDI of arm = 1.2), number average molecular weight is 910K. $PMETAI_{5.6}$ also has a number-average degree of polymerization per arm of 170 (PDI of arm = 1.2), number average molecular weight is 280K. Detailed synthesis steps and characterization was published earlier.[47]

Preparation of LbL Films and Microcapsules. PSS and PMETAI star polyelectrolyte were dissolved in 0.01 M Tris-HCl buffer (pH = 7) with the concentration of 0.2 mg/mL. PEI solution (1.0 mg/mL) in 0.01 M Tris-HCl buffer was used to deposit the prelayer. A silicon wafer was cleaned with pirana solution (3:1 concentrated sulfuric acid and hydrogen peroxide mixture. *Caution strong oxidizer!)* according to the known procedure.[84] It was then rinsed with abundant nanopure water and dried with a nitrogen stream. LbL films were prepared by the dip-assisted method: the silicon substrate was alternately immersed in PSS and PMETAI star polyelectrolyte solution for 15 min, followed by rinsing two times with 0.01 M Tris-HCl buffer. For most of the studies, we prepared LbL film with bilayer numbers of 5, 8, and 11, all of which have PSS as the outmost layer.

The preparation of LbL $(PSS/PMETAI)_n$ microcapsules is shown in Scheme 2: the bare, negatively charged silica particles with average diameter of 4 μm were first coated with a PEI prelayer by incubation in 1.5 mL of PEI solution (1.0 mg/mL) for 15 min, followed by two centrifugation (3000 rpm for 3 min)/wash cycles. Subsequently, the silica particles were incubated in 1.5 mL of PSS solution (0.2 mg/mL) for 15 min, followed by two centrifugation (3000 rpm for 3 min)/wash cycles. A 1.5 mL of PMETAI star polyelectrolyte solution was then added to the silica particles and 15 min was allowed for adsorption, also followed by two centrifugation cycles. The PSS and PMETAI star polyelectrolyte adsorption steps were repeated until the desired number of layers was built on silica particles. Hollow

microcapsules were finally obtained by dissolving silica cores in 0.5% HF solution for 2h, followed by dialysis in Nanopure water for 36h with a repeated change of water.

Atomic Force Microscopy (AFM). AFM images were obtained using a Dimension-3000 (Digital Instruments) microscope in the ``light'' tapping mode according to the well established procedure.[85,86] For capsule sample preparation, a drop of microcapsule suspension was placed onto a precleaned silicon wafer and dried in air prior to AFM imaging. Thickness of the microcapsules was determined as half of the height of the collapsed flat regions of dried microcapsules from generated height histograms by NanoScope software.[87]

Ellipsometry. Film assembly as well as thickness was determined using a M-2000U spectroscopic ellipsometer (Woollam). Prior to the measurements, samples were dried with nitrogen stream. The thickness value of the LbL film was obtained by fitting measured raw data with the Cauchy model.

UV−Visible Spectroscopy. A UV-2450 spectrophotometer (Shimadzu) was used to monitor the absorbance increments of the films on quartz slides. PSS has a maximum absorption peak at 227 nm, while PMETAI shows no absorption in the UV−vis region. Data were evaluated after the spectrum of the piranha-treated blank quartz sample was subtracted from each of the measured spectra.

Scanning Electron Microscopy (SEM). SEM imaging of hollow capsules was performed on a Hitachi S-3400-II scanning electron microscope with an electric current of 10 kV in vacuum (<1 Pa). Microcapsules air-dried on silicon wafers and were then sputter-coated with gold before imaging.

Zeta-Potential Measurements. Surface potentials of bare and coated silica particles were measured from aqueous solutions on Zetasizer Nano-ZS (Malvern). Each value of the zeta-potential was obtained at ambient conditions by averaging three independent measurements of 35 subruns each.

Confocal Laser Scanning Microscopy (CLSM). Confocal images of capsules were obtained with an LSM 510 UV−vis laser scanning microscope (Zeiss, Germany) equipped with C-Apochromat 63× oil immersion objective. The excitation/emission wavelengths were 488/515 nm. Microcapsules were visualized through the addition of fluorescein isothiocyanate (FITC) to the capsule suspension. A drop of hollow capsule suspension was added to Lab-Tek chamber (Electron Microscopy Sciences), which was then filled with 0.01 M Tris-HCl buffer. Microcapsules were allowed to settle down and then analyzed. To investigate the permeability of microcapsules, a drop of dispersion of hollow capsules was added to the Lab-Tek chamber, which was then half-filled with 0.01 M Tris-HCl buffer and then mixed with FITC-dextran solutions of different molecular weights (1 mg/mL).

Conflict of Interest: The authors declare no competing financial interest.

Acknowledgment. This work is supported by the NSF-DMR 1002810 grant. The authors are grateful to Prof. N. Kroger for providing the facility for zeta-potential measurements, and Z. Combs, K. Hu, S. Malak, and R. Davis for technical assistance. C. V. Synatschke acknowledges funding through a BayEFG scholarship and support from the Elite Network of Bavaria.

Supporting Information Available: More SEM and confocal microscopy images of $(PSS/PMETAI)_n$ microcapsules, and the morphology changes of microcapsules after adding trivalent salt and UV irradiation. This material is available free of charge *via* the Internet at http://pubs.acs.org.

REFERENCES AND NOTES

1. Stuart, M. A. C.; Huch, W. T. S.; Genzer, J.; Muller, M.; Ober, C.; Stamm, M.; Sukhorukov, G. B.; Szleifer, I.; Tsukruk, V. V.; Urban, M.; *et al*. Emerging Applications of Stimuli-Responsive Polymer Materials. *Nat. Mater.* **2010**, *9*, 101–113.
2. Wang, Y.; Hosta-Rigau, L.; Lomas, H.; Caruso, F. Nanostructured Polymer Assemblies Formed at Interfaces: Applications from Immobilization and Encapsulation to Stimuli-Responsive Release. *Phys. Chem. Chem. Phys.* **2011**, *13*, 4782–4801.
3. Zhuk, A.; Mirza, R.; Sukhishvili, S. Multiresponsive Clay-Containing Layer-by-Layer Films. *ACS Nano* **2011**, *5*, 8790–8799.
4. Kotov, N. A.; Dekany, I.; Fendler, J. H. Layer-by-Layer Self-Assembly of Polyelectrolyte-Semiconductor Nanoparticle Composite Films. *J. Phys. Chem.* **1995**, *99*, 13065–13069.
5. Lvov, Y. M.; Decher, G.; Sukhorukov, G. B. Assembly of Thin Films by Means of Successive Deposition of Alternate Layers of DNA and Poly(allylamine). *Macromolecules* **1993**, *26*, 5396–5399.
6. Lvov, Y. M.; Ariga, K.; Kunitake, T. Layer-by-Layer Assembly of Alternate Protein/Polyion Ultrathin Films. *Chem. Lett.* **1994**, 2323–2326.
7. Lvov, Y. M.; Haas, H.; Decher, G.; Möhwald, H.; Mikhailov, A.; Mtchedlishvily, B.; Morgunova, E.; Vainshtein, B. Successive Deposition of Alternate Layers of Polyelectrolytes and a Charged Virus. *Langmuir* **1994**, *10*, 4232–4236.
8. Pavlukhina, S.; Sukhishvili, S. Polymer Assemblies for Controlled Delivery of Bioactive Molecules from Surfaces. *Adv. Drug Delivery Rev.* **2011**, *63*, 822–836.
9. Johnston, A. P. R.; Such, G. K.; Ng, S. L.; Caruso, F. Challenges Facing Colloidal Delivery Systems: from Synthesis to the Clinic. *Curr. Opin. Colloid Interface Sci.* **2011**, *16*, 171–181.
10. Becker, A. L.; Johnston, A. P. R.; Caruso, F. Layer-By-Layer-Assembled Capsules and Films for Therapeutic Delivery. *Small* **2010**, *6*, 1836–1852.
11. Johnston, A. P. R.; Cortez, C.; Angelatos, A. S.; Caruso, F. Layer-by-Layer Engineered Capsules and Their Applications. *Curr. Opin. Colloid Interface Sci.* **2006**, *11*, 203–209.
12. De Geest, B. G.; Sanders, N. N.; Sukhorukov, G. B.; Demeester, J.; De Smedt, S. C. Release Mechanisms for Polyelectrolyte Capsules. *Chem. Soc. Rev.* **2007**, *36*, 636–649.
13. De Cock, L. J.; De Koker, S.; De Geest, B. G.; Grooten, J.; Vervaet, C.; Remon, J. P.; Sukhorukov, G. B.; Antipina, M. N. Polymeric Multilayer Capsules in Drug Delivery. *Angew. Chem., Int. Ed.* **2010**, *49*, 6954–6973.
14. Pavlov, A. M.; Saez, V.; Cobley, A.; Graves, J.; Sukhorukov, G. B.; Mason, T. J. Controlled Protein Release from Microcapsules with Composite Shells Using High Frequency Ultrasound—Potential for *in Vivo* Medical Use. *Soft Matter* **2011**, *7*, 4341–4347.
15. Wang, A.; Cui, Y.; Li, J.; van Hest, J. C. M. Fabrication of Gelatin Microgels by a "Cast" Strategy for Controlled Drug Release. *Adv. Funct. Mater.* **2012**, *22*, 2673–2681.
16. Antipov, A. A.; Sukhorukov, G. B.; Leporatti, S.; Radtchenko, I. L.; Donath, E.; Möhwald, H. Polyelectrolyte Multilayer Capsule Permeability Control. *Colloids Surf., A* **2002**, *198*, 535–541.
17. Yi, Q.; Wen, D.; Sukhorukov, G. B. UV-Cross-Linkable Multilayer Microcapsules Made of Weak Polyelectrolytes. *Langmuir* **2012**, *28*, 10822–10829.
18. Ye, C.; Shchepelina, O.; Calabrese, R.; Drachuk, I.; Kaplan, D. L.; Tsukruk, V. V. Robust and Responsive Silk Ionomer Microcapsules. *Biomacromolecules* **2011**, *12*, 4319–4325.
19. Lu, Z. H.; Prouty, M. D.; Guo, Z. H.; Golub, V. O.; Kumar, C.; Lvov, Y. M. Magnetic Switch of Permeability for Polyelectrolyte Microcapsules Embedded with Co@Au Nanoparticles. *Langmuir* **2005**, *21*, 2042–2050.
20. Bedard, M. F.; De Geest, B. G.; Skirtach, A. G.; Mohwald, H.; Sukhorukov, G. B. Polymeric Microcapsules with Light Responsive Properties for Encapsulation and Release. *Adv. Colloid Interface Sci.* **2010**, *158*, 2–14.
21. Katagiri, K.; Koumoto, K.; Iseya, S.; Sakai, M.; Matsuda, A.; Caruso, F. Tunable UV-Responsive Organic−Inorganic Hybrid Capsules. *Chem. Mater.* **2009**, *21*, 195–197.
22. Skirtach, A. G.; Antipov, A. A.; Shchukin, D. G.; Sukhorukov, G. B. Remote Activation of Capsules Containing Ag Nanoparticles and IR Dye by Laser Light. *Langmuir* **2004**, *20*, 6988–6892.
23. Radt, B.; Smith, T. A.; Caruso, F. Optically Addressable Nanostructured Capsules. *Adv. Mater.* **2004**, *16*, 2184–2189.
24. Skirtach, A. G.; Karageorgiev, P.; Bedard, M. F.; Sukhorukov, G. B.; Mohwald, H. Reversibly Permeable Nanomembranes

of Polymeric Microcapsules. *J. Am. Chem. Soc.* **2008**, *130*, 11572–11573.
25. Kim, J.; Lim, H.; Hwang, Y. K.; Woo, H.; Kim, J. W.; Char, K. Template-Free Uniform-Sized Hollow Hydrogel Capsules with Controlled Shell Permeation and Optical Responsiveness. *Langmuir* **2012**, *28*, 11899–11905.
26. Bedard, M. F.; Sadasivan, S.; Sukhorukov, G. B.; Skirtach, A. Assembling Polyelectrolytes and Porphyrins into Hollow Capsules with Laser-Responsive Oxidative Properties. *J. Mater. Chem.* **2009**, *19*, 2226–2233.
27. Katagiri, K.; Matsuda, A.; Caruso, F. Effect of UV−Irradiation on Polyelectrolyte Multilayered Films and Hollow Capsules Prepared by Layer-by-Layer Assembly. *Macromolecules* **2006**, *39*, 8067–8074.
28. Bedard, M.; Skirtach, A. G.; Sukhorukov, G. B. Optically Driven Encapsulation Using Novel Polymeric Hollow Shells Containing an Azobenzene Polymer. *Macromol. Rapid Commun.* **2007**, *28*, 1517–1521.
29. Antipov, A. A.; Sukhorukov, G. B. Polyelectrolyte Multilayer Capsules as Vehicles with Tunable Permeability. *Adv. Colloid Interface Sci.* **2004**, *111*, 49–61.
30. Antipina, M. N.; Sukhorukov, G. B. Remote Control over Guidance and Release Properties of Composite Polyelectrolyte Based Capsules. *Adv. Drug Delivery Rev.* **2011**, *63*, 716–729.
31. Tsitsilianis, C. Responsive Reversible Hydrogels from Associative ``Smart'' Macromolecules. *Soft Matter* **2010**, *6*, 2372–2388.
32. Jusufi, A.; Likos, C. N. Colloquium: Star-Branched Polyelectrolytes: The Physics of their Conformations and Interactions. *Rev. Mod. Phys.* **2009**, *81*, 1753–1772.
33. Genson, K. L.; Holzmueller, J.; Leshchiner, I.; Agina, E.; Boiko, N.; Shibaev, V. P.; Tsukruk, V. V. Organized Monolayers of Carbosilane Dendrimers with Mesogenic Terminal Groups. *Macromolecules* **2005**, *38*, 8028–8035.
34. Peleshanko, S.; Tsukruk, V. V. The Architectures and Surface Behavior of Highly Branched Molecules. *Prog. Polym. Sci.* **2008**, *33*, 523–580.
35. Peleshanko, S.; Gunawidjaja, R.; Petrash, S.; Tsukruk, V. V. Synthesis and Interfacial Behavior of Amphiphilic Hyperbranched Polymers: Poly(ethylene oxide)−Polystyrene Hyperbranches. *Macromolecules* **2006**, *39*, 4756–4766.
36. Gao, H.; Matyjaszewski, K. Synthesis of Functional Polymers with Controlled Architecture by CRP of Monomers in the Presence of Cross-Linkers: From Stars to Gels. *Prog. Polym. Sci.* **2009**, *34*, 317–350.
37. Peleshanko, S.; Jeong, J.; Shevchenko, V. V.; Genson, K. L.; Pikus, Yu.; Ornatska, M.; Petrash, S.; Tsukruk, V. V. Synthesis and Properties of Asymmetric Heteroarmed PEOn-b-PSm Star Polymers with End Functionalities. *Macromolecules* **2004**, *37*, 7497–7506.
38. Peleshanko, S.; Tsukruk, V. V. Assembling Hyperbranched Polymerics. *J. Polym. Sci., Part B: Polym. Phys.* **2012**, *50*, 83–100.
39. Peleshanko, S.; Jeong, J.; Gunawidjaja, R.; Tsukruk, V. V. Amphiphilic Heteroarm PEO-b-PSm Star Polymers at the Air−Water Interface: Aggregation and Surface Morphology. *Macromolecules* **2004**, *37*, 6511–6522.
40. Borisov, O. V.; Zhulina, E. B.; Leermakers, F. A. M.; Ballauff, M.; Müller, A. H. E. Conformations and Solution Properties of Star-Branched Polyelectrolytes. *Adv. Polym. Sci.* **2011**, *241*, 1–55.
41. Peleshanko, S.; Gunawidjaja, R.; Jeong, J.; Shevchenko, V. V.; Tsukruk, V. V. Surface Behavior of Amphiphilic Heteroarm Star-Block Copolymers with Asymmetric Architecture. *Langmuir* **2004**, *20*, 9423–9427.
42. Khopade, A. J.; Caruso, F. Stepwise Self-Assembled Poly(amidoamine) Dendrimer and Poly(styrenesulfonate) Microcapsules as Sustained Delivery Vehicles. *Biomacromolecules* **2002**, *3*, 1154–1162.
43. Feng, C. L.; Caminade, A. M.; Majoral, J. P.; Gu, J.; Zhu, S.; Su, H.; Hu, X.; Zhang, D. DNA Hybridization Induced Selective Encapsulation of Small Dye Molecules in Dendrimer Based Microcapsules. *Analyst* **2010**, *135*, 2939–2944.
44. Kim, B. S.; Lebedeva, O. V.; Koynov, K.; Gong, H.; Caminade, A. M.; Majoral, J. P.; Vinogradova, O. I. Effect of Dendrimer Generation on the Assembly and Mechanical Properties of DNA/Phosphorus Dendrimer Multilayer Microcapsules. *Macromolecules* **2006**, *39*, 5479–5483.
45. Addison, T.; Cayre, O. J.; Biggs, S.; Armes, S. P.; York, D. Polymeric Microcapsules Assembled from a Cationic/Zwitterionic Pair of Responsive Block Copolymer Micelles. *Langmuir* **2010**, *26*, 6281–6286.
46. MacDiarmid, A. G.; Hall, N. F. Illumination-pH Effects in Solutions of Complex Cyanides. *J. Am. Chem. Soc.* **1953**, *75*, 5204–5207.
47. Plamper, F. A.; Schmalz, A.; Penott-Chang, E.; Drechsler, M.; Jusufi, A.; Ballauff, M.; Müller, A. H. E. Synthesis and Characterization of Star-Shaped Poly(*N*,*N*-dimethylaminoethyl methacrylate) and Its Quaternized Ammonium Salts. *Macromolecules* **2007**, *40*, 5689–5697.
48. Plamper, F. A.; Walther, A.; Müller, A. H. E.; Ballauff, M. Nanoblossoms: Light-Induced Conformational Changes of Cationic Polyelectrolyte Stars in the Presence of Multivalent Counterions. *Nano Lett.* **2007**, *7*, 167–171.
49. Choi, I.; Suntivich, R.; Plamper, F. A.; Synatschke, C. V.; Müller, A. H. E.; Tsukruk, V. V. pH-Controlled Exponential and Linear Growing Modes of Layer-by-Layer Assemblies of Star Polyelectrolytes. *J. Am. Chem. Soc.* **2011**, *133*, 9592–9606.
50. Orozco, V. H.; Kozlovskaya, V.; López, B. L.; Tsukruk, V. V. Biodegradable Self-Reporting Nanocomposite Films of Poly(lactic acid) Nanoparticles Engineered by Layer-by-Layer Assembly. *Polymer* **2010**, *51*, 4127–4139.
51. Hübsch, E.; Ball, V.; Senger, B.; Decher, G.; Voegel, J.; Schaaf, P. Controlling the Growth Regime of Polyelectrolyte Multilayer Films: Changing from Exponential to Linear Growth by Adjusting the Composition of Polyelectrolyte Mixtures. *Langmuir* **2004**, *20*, 1980–1985.
52. Donath, E.; Sukhorukov, G. B.; Caruso, F.; Davis, S. A.; Möhwald, H. Novel Hollow Polymer Shells by Colloid-Templated Assembly of Polyelectrolytes. *Angew. Chem., Int. Ed.* **1998**, *37*, 2201–2205.
53. Ai, H.; Fang, M.; Jones, S. A.; Lvov, Y. M. Electrostatic Layer-by-Layer Nanoassembly on Biological Microtemplates: Platelets. *Biomacromolecules* **2002**, *3*, 560–564.
54. Lvov, Y.; Antipov, A. A.; Mamedov, A.; Möhwald, H.; Sukhorukov, G. B. Urease Encapsulation in Nanoorganized Microshells. *Nano Lett.* **2001**, *1*, 125–128.
55. Feng, Z.; Wang, Z.; Gao, C.; Shen, J. Direct Covalent Assembly to Fabricate Microcapsules with Ultrathin Walls and High Mechanical Strength. *Adv. Mater.* **2007**, *19*, 3687–3691.
56. Cavalieri, F.; Postma, A.; Lee, L.; Caruso, F. Assembly and Functionalization of DNA-Polymer Microcapsules. *ACS Nano* **2009**, *3*, 234–240.
57. Shchepelina, O.; Lisunova, M. O.; Drachuk, I.; Tsukruk, V. V. Morphology and Properties of Microcapsules with Different Core Releases. *Chem. Mater.* **2012**, *24*, 1245–1254.
58. Leporatti, S.; Voigt, A.; Mitlöhner, R.; Sukhorukov, G.; Donath, E.; Möhwald, H. Scanning Force Microscopy Investigation of Polyelectrolyte Nano- and Microcapsule Wall Texture. *Langmuir* **2000**, *16*, 4059–4063.
59. Drachuk, I.; Shchepelina, O.; Lisunova, M.; Harbaugh, S.; Kelley-Loughnane, N.; Stone, M.; Tsukruk, V. V. pH-Responsive Layer-by-Layer Nanoshells for Direct Regulation of Cell Activity. *ACS Nano* **2012**, *6*, 4266–4278.
60. Kozlovskaya, V.; Kharlampieva, E.; Drachuk, I.; Cheng, D.; Tsukruk, V. V. Responsive Microcapsule Reactors Based on Hydrogen-Bonded Tannic Acid Layer-by-Layer Assemblies. *Soft Matter* **2010**, *6*, 3596–3608.
61. Armstrong, J. K.; Wenby, R. B.; Meiselman, H. J.; Fisher, T. C. The Hydrodynamic Radii of Macromolecules and Their Effect on Red Blood Cell Aggregation. *Biophys. J.* **2004**, *87*, 4259–4270.
62. Shchepelina, O.; Drachuk, I.; Gupta, M. K.; Lin, J.; Tsukruk, V. V. Silk-on-Silk Layer-by-Layer Microcapsules. *Adv. Mater.* **2011**, *23*, 4655–4660.
63. Zhulina, E. B.; Borisov, O. V.; Birshtein, T. M. Polyelectrolyte Brush Interaction with Multivalent Ions. *Macromolecules* **1999**, *32*, 8189–8196.

64. Mei, Y.; Lauterbach, K.; Hoffmann, M.; Borisov, O. V.; Ballauff, M.; Jusufi, A. Collapse of Spherical Polyelectrolyte Brushes in the Presence of Multivalent Counterions. *Phys. Rev. Lett.* **2006**, *97*, 158301–158304.
65. Luzinov, I.; Minko, S.; Tsukruk, V. V. Adaptive and Responsive Surfaces through Controlled Reorganization of Interfacial Polymer Layers. *Prog. Polym. Sci.* **2004**, *29*, 635–698.
66. Tian, W.; Ma, Y. Molecular Dynamics Simulation of a Charged Dendrimer in Multivalent Salt Solution. *J. Phys. Chem. B* **2009**, *113*, 13161–13170.
67. Trotsenko, O.; Roiter, Y.; Minko, S. Conformational Transitions of Flexible Hydrophobic Polyelectrolytes in Solutions of Monovalent and Multivalent Salts and Their Mixtures. *Langmuir* **2012**, *28*, 6037–6044.
68. Roiter, Y.; Trotsenko, O.; Tokarev, V.; Minko, S. Single Molecule Experiments Visualizing Adsorbed Polyelectrolyte Molecules in the Full Range of Mono- and Divalent Counterion Concentrations. *J. Am. Chem. Soc.* **2010**, *132*, 13660–13662.
69. Hsiao, P.; Luijten, E. Salt-Induced Collapse and Reexpansion of Highly Charged Flexible Polyelectrolytes. *Phys. Rev. Lett.* **2006**, *97*, 148301–148304.
70. Jusufi, A.; Likos, C. N.; Löwen, H. Conformations and Interactions of Star-Branched Polyelectrolytes. *Phys. Rev. Lett.* **2002**, *88*, 018301–018304.
71. Ishikubo, A.; Mays, J.; Tirrell, M. Behavior of Cationic Surfactants in Poly(styrene sulfonate) Brushes. *Ind. Eng. Chem. Res.* **2008**, *47*, 6426–6433.
72. Angelini, T. E.; Liang, H.; Wriggers, W.; Wong, G. C. L. Like-Charge Attraction between Polyelectrolytes Induced by Counterion Charge Density Waves. *Proc. Natl. Acad. Sci. U.S.A.* **2003**, *100*, 8634–8637.
73. Nguyen, T. T.; Rouzina, I.; Shklovskii, B. I. Reentrant Condensation of DNA Induced by Multivalent Counterions. *J. Chem. Phys.* **2000**, *112*, 2562–2568.
74. Wittemann, A.; Drechsler, M.; Talmon, Y.; Ballauff, M. High Elongation of Polyelectrolyte Chains in the Osmotic Limit of Spherical Polyelectrolyte Brushes: A Study by Cryogenic Transmission Electron Microscopy. *J. Am. Chem. Soc.* **2005**, *127*, 9688–9689.
75. Tong, W.; Gao, C.; Möhwald, H. Single Polyelectrolyte Microcapsules Fabricated by Glutaraldehyde-Mediated Covalent Layer-By-Layer Assembly. *Macromol. Rapid Commun.* **2006**, *27*, 2078–2083.
76. Grosberg, A. Y.; Nguyen, T. T.; Shklovskii, B. I. Colloquium: The Physics of Charge Inversion in Chemical and Biological Systems. *Rev. Mod. Phys.* **2002**, *74*, 329–345.
77. Moggi, L.; Bolletta, F.; Balzani, V.; Scandola, F. Photochemistry of Co-ordination Compounds—XV: Cyanide Complexes. *J. Inorg. Nucl. Chem.* **1966**, *28*, 2589–2597.
78. Bédard, M. F.; Munoz-Javier, A.; Mueller, R.; del Pino, P.; Fery, A.; Parak, W. J.; Skirtach, A. G.; Sukhorukov, G. B. On the Mechanical Stability of Polymeric Microcontainers Functionalized with Nanoparticles. *Soft Matter* **2009**, *5*, 148–155.
79. Jiang, J.; Tong, X.; Zhao, Y. A New Design for Light-Breakable Polymer Micelles. *J. Am. Chem. Soc.* **2005**, *127*, 8290–8291.
80. Connal, L. A.; Li, Q.; Quinn, J. F.; Tjipto, E.; Caruso, F.; Qiao, G. G. pH-Responsive Poly(acrylic acid) Core Cross-Linked Star Polymers: Morphology Transitions in Solution and Multilayer Thin Films. *Macromolecules* **2008**, *41*, 2620–2626.
81. Tan, W. S.; Cohen, R. E.; Rubner, M. F.; Sukhishvili, S. A. Temperature-Induced, Reversible Swelling Transitions in Multilayers of a Cationic Triblock Copolymer and a Polyacid. *Macromolecules* **2010**, *43*, 1950–1957.
82. Tan, W. S.; Zhu, Z. C.; Sukhishvili, S. A.; Rubner, M. F.; Cohen, R. E. Effect of Block Copolymer Architecture on the Thermally Induced Swelling of Micelle-Containing Multilayer Thin Films. *Macromolecules* **2011**, *44*, 7767–7774.
83. Engler, A. C.; Bonner, D. K.; Buss, H. G.; Cheung, E. Y.; Hammond, P. T. The Synthetic Tuning of Clickable pH Responsive Cationic Polypeptides and Block Copolypeptides. *Soft Matter* **2011**, *7*, 5627–5637.
84. Sheller, N. B.; Petrash, S.; Foster, M. D.; Tsukruk, V. V. Atomic Force Microscopy and X-ray Reflectivity Studies of Albumin Adsorbed onto Self-Assembled Monolayers of Hexadecyltrichlorosilane. *Langmuir* **1998**, *14*, 4535–4544.
85. McConney, M. E.; Singamaneni, S.; Tsukruk, V. V. Probing Soft Matter with the Atomic Force Microscope: Force-Spectroscopy and Beyond. *Polym. Rev.* **2010**, *50*, 235–286.
86. Tsukruk, V. V.; Singamaneni, S. *Scanning Probe Microscopy of Soft Matter: Fundamentals and Practices*; Wiley-VCH: Weinheim, Germany, 2012.
87. Elsner, N.; Dubreuil, F.; Fery, A. Tuning of Microcapsule Adhesion by Varying the Capsule-Wall Thickness. *Phys. Rev. E: Stat., Nonlinear, Soft Matter Phys.* **2004**, *69*, 031802–031807.